applied sciences

MDPI

Article

A Statistical Assessment of Water Availability for Hydropower Generation in the Context of Adequacy Analyses

Giuseppe Marco Tina and Claudio Francesco Nicolosi *

Department of Electrical, Electronic and Computer Engineering (DIEEI), University of Catania, Viale Andrea Doria n.6, 95125 Catania, Italy

* Correspondence: nicolosiclaudiofrancesco@gmail.com

Abstract: The increasing presence of non-programmable renewable energy plants increases the intermittency of the electricity supply and thus threatens the adequacy of a power system. Hydropower can solve this problem due to its flexibility. This paper applies statistical approaches to assess water availability in the context of hydropower generation and adequacy analysis on a seasonal basis for one site in Sicily and the other in Sardinia, where major hydroelectric plants are present. First, an empirical relationship between soil moisture content (SMC) and potential evapotranspiration (ET0) is evaluated through linear regression analysis. Then, precipitation trends over the last twenty years are analyzed to determine any effects of global warming on water availability. Finally, Monte Carlo algorithms are used for the stochastic generation of hourly precipitation, direct runoff profiles, and daily SMC profiles. Strong positive and negative correlations between ET_0 and SMC ($p < 0.05$), and $R^2 \geq 0.5$ are found for both sites, except for summer, and $R^2 \geq 0.5$ is obtained. The cumulative pH-historical precipitation shows changes in seasonal trends, with evidence of a decrease at the annual level. The algorithms used to synthetically generate hourly precipitation and direct runoff profiles, as well as daily SMC profiles, effectively simulate the statistical variability of the historical profiles of these physical quantities.

Keywords: climate change; hydropower; adequacy; Monte Carlo; water availability; direct runoff; linear regression; soil physics

check for updates

Citation: Tina, G.M.; Nicolosi, C.F. A Statistical Assessment of Water Availability for Hydropower Generation in the Context of Adequacy Analyses. *Appl. Sci.* **2023**, *13*, 1986. https://doi.org/10.3390/app13031986

Academic Editor: Alberto Benato

Received: 20 December 2022
Revised: 31 January 2023
Accepted: 31 January 2023
Published: 3 February 2023

Copyright: © 2023 by the authors. Licensee MDPI, Basel, Switzerland. This article is an open access article distributed under the terms and conditions of the Creative Commons Attribution (CC BY) license (https://creativecommons.org/licenses/by/4.0/).

1. Introduction

1.1. European Energy Sector Emissions and EU Actions to Counter Them

In climate science, the climate system is defined as the whole of the atmosphere, the hydrosphere, the cryosphere, the biosphere, and the land surface [1]; thus, the climate is the state of the climate system [2]. Furthermore, climate change can be defined as a statistically significant variation in climate from its mean state or its variability. The large variations in the current climate are likely due to human activities, which by causing an increase in the greenhouse gas (GHGs) concentrations in the atmosphere, trigger a change in climate [3]. Specifically, different human sectors emit significant percentages of carbon dioxide into the atmosphere, and to set a figure, referring to the energy sector in 2021 global energy-related CO_2 emissions were 33.0 Gt [4].

It is worth dwelling on some data pertaining to the European Union (EU). In the EU the two sectors that experience the highest CO_2 emissions are energy supply and transport [5]. However, defining the CO_2 emission intensity as the ratio between the CO_2 emissions due to electricity generation and gross electricity generation [6], since 1990 the intensity of GHGs emissions from electricity generation has decreased markedly, reaching, an amount of CO_2 emitted by half of that emitted in 1990 for 1 kilowatt hour generated in 2020. This sharp decrease is mainly due to the high number of investments and installations of renewable energy systems. Indeed, in the decade 2009–2019, solar photovoltaics (PV), wind power, and solid biofuels, have driven the growth of renewable energy in the EU [7].

Although the installed capacity of hydropower had only a slight increase in the decade 2009–2019 [8], wind and hydropower made up two-thirds of the total electricity generated from renewable energy sources (RES) in 2019 [7]; the remaining one-third was covered by PV (13%), solid biofuels (8%) and other RES (9%). Although the 13% (125.7 TWh) share of generation by PV as of 2019 may seem small, it must be considered that this generation technology started from a 1% (7.4 TWh) share in 2008; this sharp percentage increase over a decade makes PV technology the one with the fastest growth rate among all renewables in EU.

The data cited above testify to a trend in the penetration of renewables, in the generation mixes of EU countries' electric power systems (EPSs), that is set to increase further to meet the environmental targets of net zero GHGs emissions by 2050. Indeed, in 2019 the EU released the European Green Deal [9], an agreement among the member countries to achieve sustainable development goals, such as GHGs emission reductions of 55% below 1990 levels by 2030, and climate neutrality by 2050. To achieve these challenging goals, the EU plans to focus heavily on PV and wind power installations. It is worth mentioning a recent energy plan, also released by the EU, namely the REPowerEU Plan [10], which aims to increase the installation rates of wind and PV power plants already envisioned by [11]. Energy savings, heat pumps, renewable hydrogen, biomethane, and electrification of industrial sectors currently fossil-fueled, are the other linchpins of the European strategy.

An ever-increasing amount of renewable generation sources in the power systems of EU countries (and beyond) poses risks to system adequacy, and therefore the flexibility of other generation sources already present in the EPSs of the respective countries, along with storage, is crucial to the proper functioning of present and future power systems, as is illustrated in the following subsections.

1.2. Interaction between Climate Change and Power Systems

The increasing presence of RES in the generation mixes of European and non-European electric power systems is, on the one hand, reducing the impact of power generation in terms of CO_2 released into the atmosphere, but on the other hand, it is jeopardizing the adequacy of power systems [12]. This is happening because the energy produced by nonprogrammable renewable sources (PV, wind power) [13–15], along with their efficiencies [13], depends on the dynamics of weather variables, which are inherently stochastic (i.e., it is not possible to predict a priori, instant by instant, the values assumed by weather variables). In turn, global warming is and will increasingly threaten the adequacy and safety of power systems.

It follows from the above considerations that it is becoming increasingly pressing to analyze the impacts of current and future climate on current and future power systems. The most characteristic aspect of these analyses, however, is uncertainty: climate models' projections of future climate are affected by uncertainty due to climate dynamics; the impact of future power generation technologies on GHGs concentrations in the atmosphere, cannot be known a priori [13]; the impact of future climate on future EPS is characterized by the double uncertainty given by future climate change projections and the energy policies of different countries [16]. These uncertainties occur on both a spatial and temporal basis. The inherent presence of uncertainty in the above analyses suggests how statistical approaches can reliably model the impacts of climate on energy production and demand.

Climate change is already increasing the frequency, severity, and persistence of extreme weather events, thereby impacting the resilience and reliability of electric power systems [17]. Furthermore, climate change is characterized by marked spatial variability, on a regional scale; for example, the Mediterranean region will be one of the most affected by the effects of climate change in the coming decades, with temperature increases of 20% above the global average, and a marked reduction in the amount of annual precipitation [18]. This spatial variability in the effects of climate change has immediate consequences for electricity production and demand: the European continent will experience polarized global warming effects on thermoelectric and hydroelectric generation between northern

and southern Europe [19]. Going into the specifics of individual countries, Italy would experience a general decrease in available PV and wind generation, and a sharp decrease in thermoelectric generation and efficiency [13,19].

In this framework, climate model projections can be useful in evaluating the level of production and efficiency of future generation plants, as well as future electricity demand. In this regard, one paper shows that a +2 °C increase in average temperatures would impact future European electricity generation and demand more markedly than a +1.5 °C increase [20].

In this paper, climate models are not used; rather, statistical techniques are applied to simulate time series of meteorological and hydrological variables that directly influence the amount of water available for hydropower production, whether from run-of-the-river or reservoir systems.

1.3. The Role of Hydropower on the Adequacy of Power Systems

Since adequacy is the ability of an EPS to meet energy demand at any given time and market area in a given country, and since nonprogrammable sources are stochastically dependent on trends in weather variables, today's power systems are experiencing increasing precariousness in deterministically meeting load demand. Exacerbating this picture is the energy crisis sweeping the EU in the wake of geopolitical unrest in Eastern Europe. This crisis is not only about the commodity prices of electricity and gas in their respective markets, but also regards the terms of the availability of fuels for power generation and the consequent compliance with the adequacy levels of European power systems [21].

Different solutions and different approaches can be devised to deal with the above issues and challenges, but hydropower can already be considered one of the main reliefs to the risks of the inadequacy of an EPS [22]. In fact, hydropower is not only an important renewable energy source for several countries around the world, capable of covering both base loads and peak demand, but can be a useful source of relief for grid imbalances between generation and demand. In cases of grid imbalance, hydropower plants are among the fastest in terms of start-up time when there is a generation shortfall in demand coverage [23]. This implies that flexible hydropower management can facilitate the integration of non-programmable renewable energy into EPSs. Going into national detail, a study conducted on the Spanish power system, and future energy scenarios in this country, shows how flexible hydropower management can play an important role in generation fleet adequacy, reducing power shortages [24].

Taking advantage of the flexibility of hydropower technology, however, involves meeting both operational constraints (on the security of supply) and governmental and environmental constraints (on reservoir levels and river flows). Thus, modeling regarding hydropower involves consideration of all aspects underlying the interaction between hydropower and the power systems [25]. Among these aspects is the modeling of water availability, and thus water inflow to hydropower plants, which has seasonal variability.

1.4. Literature Review (Analysis) of the Impact of Climate Variables on Hydropower Generation

Despite the importance of hydropower generation to the adequacy of a power system, there is, to the author's knowledge, little literature that addresses modelling the impact of climate variables on hydropower generation (both run-of-river and storage) with respect to the adequacy of a power system [26]. The most important aspect of adequacy analyses is that they are carried out using statistical methods based on probability theory and stochastic modelling of generation and demand profiles. In this context, there is a lack of work in the literature that models synthetic profiles of meteorological and hydrological variables for the purpose of adequacy analyses. The study and theorising of these types of models are crucial today but will become even more important in the future as trends in weather variables continue to change due to climate change.

This paper attempts to fill the gap in the literature. First, linear regression is used to search for empirical relationships linking soil moisture (expressed as soil water content saturation fraction) and potential evapotranspiration, which is evaluated for a reference crop for specific geographical locations. The purpose of this evaluation is that daily time series of potential evapotranspiration can be derived from the soil moisture data. Since precipitation is the main driver of the hydrological cycle, hourly precipitation trends are analysed next. This can be useful because while the direction of the impact of global warming on air and ocean temperature trends is well known, the direction of the impact on precipitation is still a subject of scientific debate [27,28]. Furthermore, the analysis of precipitation trends allows conclusions to be drawn about the development of water availability for hydropower plants. This is because the main source of water availability for a power plant is direct runoff, which in turn results from precipitation. For this reason, two models from the literature are presented here that can be used to assess direct runoff: one model considers only the precipitation intensity (mm/h), while the other includes the daily precipitation amount (mm). Since adequacy analyses are carried out with statistical approaches [12], this work also uses the Monte Carlo method for the stochastic generation of hourly precipitation and direct runoff profiles as well as daily soil moisture profiles. In this way, synthetic profiles are obtained that form the building blocks on which simulations of hydropower generation profiles can be built for future research. Finally, to complement the analyses just described, additional physical considerations are added to the assumptions and considerations.

All simulations are performed in MATLAB.

The paper is organized as follows: Section 2 explains in detail the methodologies implemented, the results of which are in Section 3. Section 4 provides final considerations on the methodologies and the results obtained.

2. Methodologies

This section presents, in addition to an introductory subsection of the physics of a catchment, the methodologies and procedures applied for: the evaluation of empirical relationships between potential evapotranspiration and SMC through linear regression; the analysis of seasonal and annual precipitation trends over the past twenty years; application of Monte Carlo approaches for generating synthetic profiles of precipitation, direct runoff, and SMC. Satellite data of hourly precipitation (mm/h) and of daily (hourly values are not currently available) soil moisture content (SMC), expressed as soil saturation fraction (dimensionless), are used; these data are taken from the MERRA-2 product, one of the NASA's databases having a spatial resolution of $0.5^\circ \times 0.625^\circ$ (latitude and longitude, respectively) [29].

2.1. The Hydrology of a Catchment, Basic Concepts

The water balance of a catchment area is influenced by the amount and intensity of precipitation, evapotranspiration, and runoff, as well as the change in moisture stored in the soil [30]. Precipitation is one of the main sources of water for the catchment; depending on its intensity (mm/h) and its amount (mm), variates the fraction of water that will seep into the ground or runoff into the river or into the basin.

However, not all of the atmospheric precipitation reaches the ground surface; in fact, depending on the type of crop and vegetation canopy, some of the precipitation is intercepted and evaporates without ever having reached the ground [31]. Precipitation that does not remain intercepted in the foliage and reaches the soil surface will infiltrate, evaporate, or runoff, depending on climatic conditions (net radiation, air temperature, wind speed, and relative humidity) and soil types and conditions. In fact, depending on the soil texture, the physical properties of the soil change; these include field capacity, saturation capacity, permanent wilting point, and available water capacity [32].

The saturation capacity is reached when all pores are filled with water; however, in this condition, gravity drains some of the water into the lower layers of soil. The amount of water that remains after this drainage is the field capacity of the soil. However, the field capacity does not correspond to the total amount of water available in the soil (available water capacity). In fact, a fraction of the field capacity is bound to solid soil particles by capillary forces and is available neither for evapotranspiration nor for plant nutrition; this amount of water is called the permanent wilting point [33]. Finally, taking away the wilting point, the remaining water percentage of the field capacity is water that is free to move, that is, available water [33].

The texture of the soil, together with the amount of moisture (water) in the soil, characterize the infiltration capacity of the soil. When atmospheric precipitation phenomena occur, if the soil is saturated or if the intensity of precipitation is greater than the infiltration rate, the amount of precipitation that reaches the soil will constitute direct runoff that will feed the river or basin near the catchment.

In hydrology, the soil is usually divided into two zones, one called unsaturated, and the other called saturated, separated by an imaginary line called the water table. The water stored in the unsaturated zone is called soil water [34], and this zone is further divided into two zones: the rooting zone and the intermediate zone. The saturated zone, on the other hand, lies below the unsaturated zone and is bounded by two different layers: an upper layer that is the capillary fringe (located at the water table level) and an impermeable bottom that is the bedrock [31].

Precipitation contributes to runoff when its intensity or duration is such that it exceeds the infiltration capacity of the soil and thus surface runoff, also called direct runoff, results. Another water contribution to a catchment also comes from indirect runoff, that is, some of the water that infiltrates into the soil will percolate into the lower layers of the soil until it reaches the saturated zone, going to form groundwater. Some of this water will go into the catchment, constituting indirect runoff.

In this work, the rooting zone is considered, since it constitutes a large part of the unsaturated zone, and as such allows for modelling and consideration of fundamental aspects of soil physics that influence evapotranspiration and direct runoff [35]. The SMC data for the root zone are taken from [29], where they refer to a soil depth ranging from the surface to 100 cm. The saturated soil zone, and thus the indirect runoff are ignored in this study. This, however, is a conservative consideration, being that indirect runoff would constitute more water available for hydropower generation.

The meteorological and hydrological quantities, discussed so far, are linked together through the water balance equation, referred to as an atmosphere-land surface system. Indeed, considering that for a given time frame the hydrologic cycle as a closed system, the physical principles of conservation of energy and mass apply. In the case of water, the conservation of mass and energy posits the following expression [31]:

$$\mathrm{P} \pm \mathrm{ET} \pm \mathrm{R} = \pm \Delta \mathrm{S} \tag{1}$$

where P denotes precipitation, ET evapotranspiration, R runoff, and ΔS is the change in water stored in the soil (deep groundwater is included). The symbol $\pm$ is used in the first member of (1) to indicate how the physical quantities can be a gain or a loss for the system, depending on the reference: for the atmosphere, the ET is a gain, while for soil hydrology, it is a loss. Since the hydrological point of view is applied in this paper, (1) leads to the following:

$$\mathrm{P} - \mathrm{ET} - \mathrm{R} = \pm \Delta \mathrm{S} \tag{2}$$

The first-member terms are the main constituents of a water availability study, and therefore will be discussed in the next subsections.

2.2. Seasonal Empirical Relationships between Potential Evapotranspiration and Soil Moisture Content

The amount of potential evapotranspiration (ET_0) depends on net radiation, air temperature, relative humidity (RH), and wind speed. For example, with the same wind speed and RH, the rate of ET_0 will increase as net radiation and air temperature increase. This in turn leads to a change in the amount of water (moisture) contained in the soil. Indeed, potential evapotranspiration ET_0 (mm/day) and SMC (dimensionless) depend on the same climate variables (net insolation, air temperature, wind speed, relative humidity). These physical considerations then lead to an attempt to find empirical relationships that link ET_0 to soil moisture content, for the two geographic case studies and time frame (daily). The approach used is that of linear regression and is conducted on a seasonal basis, for each of the selected years of historical data. The purpose is to see if the coefficients of the fitting curves have consistency of magnitude and sign between the two different geographical locations chosen, over the four seasons considered, so that through fitting curve expressions, ET_0 rates (mm/day) can be directly estimated from soil moisture data (known from [29]). A first-degree polynomial is used as fitting curve.

ET_0 values are not available in [29] and therefore must be derived. The rate of evapotranspiration depends not only on atmospheric factors, but also on the type of vegetation covering the surface. Thus, several works in literature evaluate evapotranspiration depending on the type of crop considered; some papers evaluate the evapotranspiration in case of a reference crop, with the following characteristics [36]: a fixed surface resistance of 69 s/m, a fixed height of 0.12 m, and an albedo of 0.23. Furthermore, it is an extensive surface cover that completely shadows the ground [36].

In this paper, the reference crop approach is used since it makes the results found comparable with other studies using reference crop, and since ET_0 for a specific crop can be assessed through crop coefficients available in the literature. In the literature, among the models used to assess reference crop ET_0, there is one recognized by the Food and Agriculture Organization (FAO): the Penman-Monteith formula (FAO56) [37], that allows ET_0 to be evaluated on a daily basis. However, this formula requires as inputs environmental data that are not present in common in situ weather stations or satellite measurements, thus making it difficult to implement the FAO56 in several geographical regions, especially in developing countries.

Another model allows daily ET_0 estimates to be obtained close to those of FAO56 is that of Hargreaves-Samani (HS) [38], as described in [39–41]. The equation for this model requires maximum and minimum air temperature as the only climate data. The HS equation is reported below [40]:

$$ET_0 = C_1 \cdot R_{ext} \cdot (T + 17.8) \cdot \Delta T^{C_2} \left(\frac{mm}{day} \right) \quad (3)$$

where ET_0 (mm/day) is the reference potential evapotranspiration, C_1 is a constant equal to 0.0023, C_2 is another constant equal to 0.5, and ΔT (°C) is the difference between the monthly average daily maximum and minimum temperatures; the sum of these two temperature values, divided by two, yields T (°C), which is thus an average temperature; R_{ext} (mm/day) is the extraterrestrial radiation expressed in equivalent water evaporation; finally, 17.8 is an empirical factor introduced to account for the temperature units used in the original formulations. In (3) in addition to explicitly appearing atmospheric quantities on which ET_0 depends, ET_0 binding to RH is also expressed, implicitly, since ΔT depends linearly on relative humidity [42].

A specific formula must be used to evaluate R_{ext} [36]:

$$R_{ext} = C_3 \cdot d_r \cdot (\omega_s \sin\phi \sin\delta + \cos\phi \cos\delta \sin\omega_s) \left(\frac{mm}{day} \right) \quad (4)$$

where C_3 is a constant equal to 15.392; d_r (dimensionless) is the relative distance between the Sun and the Earth; ϕ (radians) is the latitude of the site; δ (radians) is the solar declination; ω_s (radians) is the sunset hour angle. The d_r, ω_s, and δ are expressed by [36]:

$$d_r = 1 + 0.033 \cdot \cos\left(\frac{2\pi}{365} J\right) (\text{dimensionless}) \quad (5)$$

where J is the Julian day number of the year.

$$\delta = 0.4093 \cdot \sin\left(\frac{2\pi}{365} J - 1.405\right) (\text{radians}) \quad (6)$$

$$\omega_s = \arccos(-\tan\phi \cdot \tan\delta) \ (\text{radians}) \quad (7)$$

2.3. Precipitation Data Assessment and Models for Water Availability in Hydropower Plants

Since precipitation is the prime driver of a catchment's hydrologic cycle and water availability for hydropower production, it is useful to conduct an analysis of historical hourly precipitation profiles for the geographic locations of interest. The months constituting the seasons are aggregated as usually done in the literature [43]: December-January-February (DJF) for winter, March-April-May (MAM) for spring, June-July-August (JJA) for summer, September-October-November (SON) for autumn. This analysis aims to understand whether the trend of hourly rainfall in recent years may positively or negatively impact the availability of water for hydropower generation. In addition, it may be interesting to observe what the effects of climate change may be on trends in extreme precipitation events. There is no univocal definition of extreme precipitation in the literature, and this paper considers extreme precipitation to be precipitation intensity greater than 3.6 mm/h, as defined in [44].

Direct runoff is proportional to the amount of water that precipitates. Thus, analysis of precipitation trends over the past twenty years also allows conclusions to be drawn about the amount of direct runoff. There are two main methods for evaluating direct runoff from precipitation: the Rational method, and the Natural Resources Conservation Service (NRCS) method [31].

The Rational method considers the intensity of precipitation (mm/h), the recurrence time of precipitation with certain intensities, and the specific catchment area considered (km^2), as shown by the following equation [31]:

$$Rf = c \cdot Pi \cdot A\left(\frac{mm \cdot km^2}{h}\right) \quad (8)$$

where Rf is the direct runoff; c is called the *runoff coefficient* and varies according to the type of land cover and slope of the land (dimensionless); Pi is the intensity of precipitation (mm/h); and A is the extent of the drainage area (km^2). To obtain the direct runoff in Equation (8) with units equal to m^3/s, one must multiply (8) by 0.278, which is thus a conversion factor. Regarding the runoff coefficient, the values of c referring to grassland (land cover assumed for ET_0 evaluation) and for different land slopes, are given in the following Table 1 [31]:

Table 1. Runoff coefficient values in the case of grassland.

Slope Grass Cover (%)	c Range
0 ÷ 5	0.10 ÷ 0.40
5 ÷ 10	0.16 ÷ 0.55
10 ÷ 30	0.22 ÷ 0.60

The main limitation of the Rational method is that the considered drainage area should not exceed 0.8 km^2, so this value is here set for A.

The NRCS method estimates, not the flow rate, but the amount of water available as runoff (mm) [45]. This method, unlike the Rational one, uses the cumulative amount of precipitation (mm) as input. The equation that 'converts' this amount to runoff is as follows [45]:

$$Rf' = \frac{(Pr - I_a)^2}{Pr - I_a + S}(mm) \quad (9)$$

where Pr (mm) is the cumulative precipitation of a day; I_a (mm), known as initial abstraction, is the loss of water to runoff due to infiltration, interception, and storage of water in surface depressions; S (mm) is the maximum potential retention after runoff begins. I_a and S are related by the following empirical relationship [45]:

$$I_a = 0.2 \cdot S(mm) \quad (10)$$

S, in turn, is evaluated by the following formula [31]:

$$S = \left(\frac{1000}{CN} - 10\right) \cdot 25.4(mm) \quad (11)$$

where CN (dimensionless) is the runoff curve number, that is, a numerical coefficient that depends on the total precipitation (both duration and intensity), soil moisture status prior to precipitation, soil type, land cover type, and temperature. These meteorological and hydrological variables that influence the values of CN, and thus the resulting runoff, are called Antecedent Runoff Conditions (ARC) and are divided into three classes: ARC I (dry conditions), ARC II (average conditions), and ARC III (wetter conditions) [45,46]. In this paper, it is assumed the ARC II class is valid. The values of CN in the case of grassland and different types of soil texture take the following values [31]: CN = 39 for sands, CN = 61 for loams, CN = 74 for clay loams, and CN = 80 for clays.

2.4. Monte Carlo Approaches for Synthetic Generation of Hourly Profiles of Precipitation and Runoff, and Daily Profiles of Soil Moisture Content

Analyses of power generation from both programmable and non-programmable renewable sources requires stochastic modeling. In the case of hydropower generation, the generation of synthetic time series of meteorological and hydrological variables, for stochastic water availability assessments, go in this direction. In this paper, the Monte Carlo method is used to generate hourly synthetic profiles of precipitation and runoff, along with daily SMC profiles; the latter have a daily resolution since no hourly resolution is available for them in [29]. The Monte Carlo approach is chosen since it lends itself well to the stochastic simulations applied in this work, in which the number of variables makes the computational weight acceptable. In addition, ENTSO-E and several transmission system operators (including Italy's Terna) apply adequacy analyses using the Monte Carlo approach; however, they use the Monte Carlo method for the stochastic generation of availability profiles, whereas in this work Monte Carlo is used for the stochastic generation of time series of meteorological and hydrological quantities.

Synthetic hourly precipitation profiles (mm/h) are evaluated by fitting a probability distribution over the twenty years of available data; specifically, a family of Pearson distributions is chosen, from which a single distribution identified through the mean, standard deviation, kurtosis, and skewness of the historical data series is selected. Random numbers are then extracted according to the distributions thus identified, and synthetic hourly precipitation series are obtained as output. This procedure is repeated using each year of historical data as a basis for each season; in this way, the inter-seasonal variability of precipitation trends is considered. Specifically, to simulate the inter-annual variability of precipitation trends, the algorithm implemented in this paper randomly chooses a single

year from the twenty years of data, and the just described fitting and extraction procedure is applied to it.

Once the synthetic hourly precipitation hourly profiles are obtained, at each Monte Carlo simulation, they are put as inputs into Equations (8) and (9), thus also obtaining synthetic direct runoff profiles.

Regarding SMC data, they are expressed in saturation fractions (range from zero to one), with one indicating a soil completely saturated. Compared to the stochastic generation of hourly precipitation profiles, a different Monte Carlo algorithm is used for the generation of synthetic daily profiles of SMC. In fact, SMC synthetic profiles are generated through inverse and bootstrap methods together. Specifically, the implemented algorithm starts by deriving an empirical cumulative distribution function (ECDF) of the historical SMC data; then, numbers belonging to the interval (0,1) are randomly generated according to a uniform distribution ($U(0,1)$). This set of random numbers is then placed as input to the inverse of the ECDF before being obtained, thus obtaining synthetic SMC profiles as outputs. Finally, from this set of synthetic SMC values, a number of elements equal to the number of days of the different seasons are sampled with replacement. As with synthetic precipitation profiles, in the case of SMC profiles, the algorithm randomly extracts one of twenty years of historical data in each simulation run; fifty Monte Carlo simulations are repeated for SMC profiles as well.

To assess the goodness of the approaches used, two error indices expressed by the following formulas are evaluated:

$$e_{mean} = \left| \frac{m_{syn} - m_{his}}{m_{syn} + m_{his}} \right| \text{(dimensionless)} \quad (12)$$

$$e_{STD} = \left| \frac{s_{syn} - s_{his}}{s_{syn} + s_{his}} \right| \text{(dimensionless)} \quad (13)$$

where in (12) m_{his} (mm/h) is the sample mean of the historical seasonal hourly profile of the randomly chosen year and m_{syn} (mm/h) is the sample mean of the corresponding synthetic seasonal hourly profile; in (13) s_{his} (mm/h) is the sample standard deviation (sample std) of the historical seasonal hourly profile and s_{syn} (mm/h) is the sample std of the corresponding synthetic seasonal hourly profile. Finally, fifty Monte Carlo simulations are carried out, for each of which the indices (12) and (13) are calculated.

2.5. Geographical Locations Case Studies

The search for geographic locations to use for the case study is conducted by considering: areas where hydropower plants are present; areas afferent to the most important rivers in a given region; areas whose crop type is grassland, with sparsely forested areas; and geographic areas where snowfall is rare, since snow and its effects on the water balance of a catchment are here ignored. The methods described in the subsections above are applied to two geographical locations in the Italian regions of Sicily and Sardinia, respectively, shown in Figure 1.

The two sites selected are near Paternò (Sicily) and near Busachi (Sardinia), whose geographical position is 37°53′47″ N longitude 14°86′14″ E and 40°01′97″ N and 8°84′85″ E, respectively. Both sites are located in catchments of the main rivers of the two islands (in terms of catchment size), namely the Simeto (Sicily) and the Tirso (Sardinia). In addition, the sites are located near hydroelectric power plants (dams), which are among the largest hydroelectric power plants on the two islands in terms of installed capacity. The soil type in both localities is loam, and the vegetation cover type is pasture, with rare and small woodland clusters. This implies that the interception of precipitation by foliage does not decisively impact the relationship between precipitation and runoff. Satellite data reveal that the geographic site chosen for Sicily has slightly higher soil moisture saturation rates than the site in Sardinia. This is probably due to the amounts of annual precipitation, which are greater for the Sicilian site. The sites are affected by a Mediterranean climate where

snowfall is very rare. This complies with the modelling of water availability, as snow and its impact on the hydrological cycle are neglected in this work.

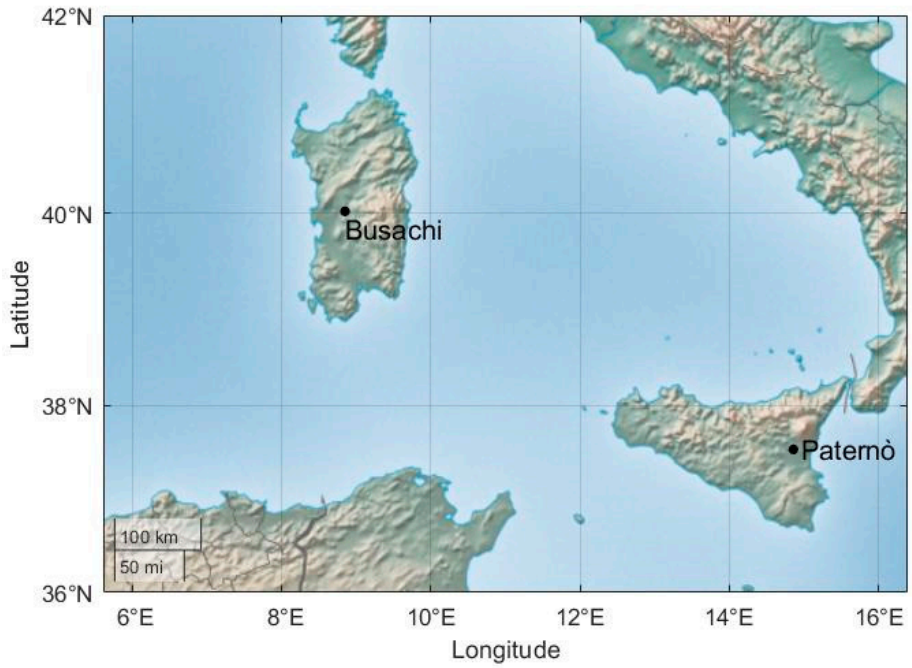


Figure 1. Map showing the geographical locations of the two Italian case studies Paternò (Sicily) and Busachi (Sardinia).

2.6. Further Physical Considerations of General Utility

The amount of water that the soil can hold in the unsaturated zone depends on the porosity of the soil, which in turn depends on the soil texture. In fact, porosity is defined as the ratio of pore volume to total soil volume [34]; thus, once the texture of the soil is known, its porosity value can also be known [47]. It follows from the above definition that porosity is related to the amount of water contained in the soil. In fact, the soil is saturated when all the water fills the pore space, so denoting θ_{ST} as the volumetric water content (VWC) of the soil at saturation (unsaturated zone), θ_{ST} coincides with porosity. As a consequence, field capacity and the permanent wilting point are specific fractions of θ_{ST}, and thus of porosity [33,47]; the value of this fraction, depends on the soil texture.

The ET at first member of (2) (Section 2.1) is actual evapotranspiration, that is, it is also related to the amount of water in the soil. In fact, given the type of land cover and soil texture, evapotranspiration increases (decreases) as SMC increases (decreases), all other atmospheric variables being equal. However, the evapotranspiration evaluated through the equations in Section 2.2 does not consider the amount of water in the soil. Due to this, it is therefore necessary to estimate the actual evapotranspiration, $ET_{0,ACT}$, by tying potential ET_0 to the VMC. For this purpose, the following function is introduced here:

$$\frac{ET_{0,ACT}}{ET_0} = \min\left\{\max\left[\frac{\theta - \theta_{WP}}{\theta_{FC} - \theta_{WP}}, 0\right], 1\right\} (\text{dimensionless}) \quad (14)$$

where the first member is the ratio of the actual ($ET_{0,ACT}$) to potential evapotranspiration (ET_0), and at second member θ is the VMC; θ_{FC} is the VMC corresponding to the field capacity and θ_{WP} is that corresponding to the wilting point. Knowing ET_0 from Equation (3) and evaluating the ratio in (14), for daily values of θ, it is possible to obtain the values of $ET_{0,ACT}$.

Some hydrological considerations are worth drawing attention to:

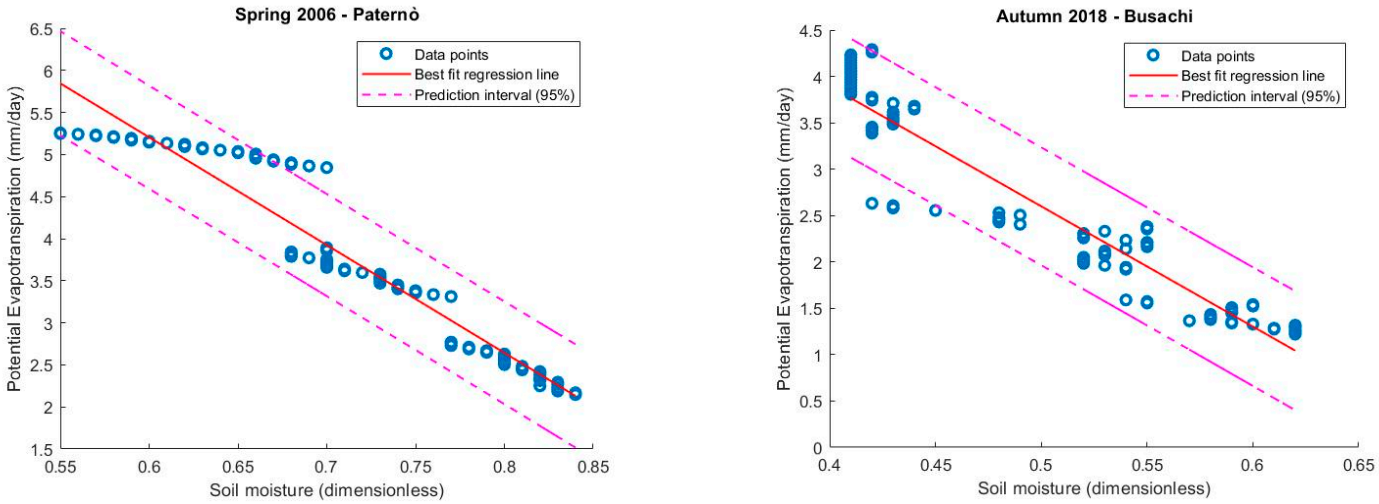
- If the hydrological cycle was annual (rather than seasonal), then it would be possible to estimate approximately ET (2) as the difference between precipitation and runoff, being that SMC has annual cycles;
- From the perspective of hydropower generation, field capacity is useful water, being that more water causes both surface runoff and groundwater recharge;
- Since ET_0 is here calculated for grassland, the stomatal control of leaves does not come into play in the relationship between ET_0 and actual evapotranspiration [34]. This physical aspect of grassland implies that the relationship between $ET_{0,ATC}$ and ET_0 is largely given by the water content of the soil;
- In applying the methodologies described in this section some assumptions were implicitly made: over the several years of simulations conducted, human land use does not change, and no mining of groundwater is carried out.

3. Results

Twenty years of historical data (from December 2001 to November 2021) of hourly precipitation and daily SMC time series are taken from [22], for the two sites of interest. Hourly values of SMC are currently (as of 2022) not available in [22]. The following subsections illustrate the results obtained through the methods described in Section 2.

3.1. Linear Regression

A polynomial of the first degree is chosen as the fitting curve, with the coefficient of determination R^2 evaluated for each season and year of the data for both sites. In addition, Spearman's correlation coefficient (S) is used to quantify the magnitude and sign of the relationship between the ET_0 calculated through the HS formula and the SMC data. Figure 2a,b shows two examples of the results obtained for the Paternò and Busachi case studies, respectively (95% prediction intervals are also shown). Instead, the Table 2a,b shows the mean, median, and standard deviation (STD) of the statistical quantities of interest for the two selected case studies.



(**a**) (**b**)

Figure 2. Fitting lines data points of soil moisture values versus potential evapotranspiration values for spring 2006 in Paternò (**a**) and autumn 2018 in Busachi (**b**). Additionally, plotted in purple are the 95% prediction intervals.

Table 2. (a) Mean, median, and standard deviation (STD) of the correlation coefficients (Corr), coefficients of determination R^2, and the slope of the fitting line, and its intercept, for the Paternò case study. (b) Mean, median, and standard deviation (STD) of the correlation coefficients (Corr), coefficients of determination R^2, and the slope of the fitting line, and its intercept, for the Busachi case study.

(a)

	Winter				**Spring**			
	Corr	**R^2**	**Slope**	**Intercept**	**Corr**	**R^2**	**Slope**	**Intercept**
Mean	0.684	0.561	4.404	−1.689	−0.928	0.855	−16.169	14.203
Median	0.735	0.545	3.255	−0.983	−0.943	0.866	−14.808	13.813
STD	0.188	0.244	2.848	2.004	0.070	0.089	5.744	2.750
	Summer				**Autumn**			
	Corr	**R^2**	**Slope**	**Intercept**	**Corr**	**R^2**	**Slope**	**Intercept**
Mean	0.006	0.120	−1.106	6.518	−0.850	0.715	−18.518	12.245
Median	−0.073	0.060	−1.853	6.742	−0.875	0.749	−15.841	11.007
STD	0.352	0.149	5.078	2.242	0.106	0.155	8.610	3.964

(b)

	Winter				**Spring**			
	Corr	**R^2**	**Slope**	**Intercept**	**Corr**	**R^2**	**Slope**	**Intercept**
Mean	0.655	0.478	6.997	−2.589	−0.783	0.654	−25.414	17.405
Median	0.719	0.468	6.905	−2.451	−0.861	0.718	−24.403	18.279
STD	0.164	0.233	3.084	1.595	0.197	0.264	6.635	3.172
	Summer				**Autumn**			
	Corr	**R^2**	**Slope**	**Intercept**	**Corr**	**R^2**	**Slope**	**Intercept**
Mean	0.352	0.196	3.221	4.420	−0.758	0.612	−21.693	11.880
Median	0.412	0.120	2.408	4.842	−0.761	0.585	−20.700	11.647
STD	0.367	0.203	5.218	2.169	0.153	0.186	7.289	2.719

From the above tables, the seasonal results of the correlation coefficient statistics for the Paternò locality are consistent in magnitude and sign with those for the Busachi locality, except for the summer: in winter, ET_0 and SMC are related by a strong positive correlation ($p < 0.05$), while in spring and autumn, a strong anticorrelation is found ($p < 0.05$); in summer, a strong variability is found, going from positive to negative values ($p < 0.05$ or $p > 0.05$ depending on the year). Finally, the anticorrelation values in autumn are lower in modulus than in spring, probably due to the approaching winter.

Regarding R^2 values, high and consistent values are obtained between the two locations, especially in spring and autumn: in these seasons, more than 60% of the variability of ET_0 is explained by the variability of SMC values. In winter this percentage drops to 50% but is still significant. Low R^2 values are obtained in summer, confirming the poor fitting that is obtained with a straight line for this season.

The coefficients of the fitting lines show the consistency of magnitude and sign in the respective seasons over the twenty years of data, in the same case study and between the two case studies (except in summer). Moreover, the intervals of the values of the slopes and intercepts of the fitting lines of the two case studies have values in common.

The statistical significance of the above results suggests that through the fitting lines found here, ET_0 values close to those of the HS formula can be obtained from the SMC data (satellite or in situ).

3.2. Precipitation Trends

Among the various precipitation trends, along with their intensities, analyzed in this work (as described in Section 2.3.), significant ones are shown here, which may give indications of what precipitation trends might look similar in the years to come. First, trends related to the Paternò locality are shown, and then later those related to Busachi. Figure 3 shows the annual cumulative precipitation trends for the Sicilian location.

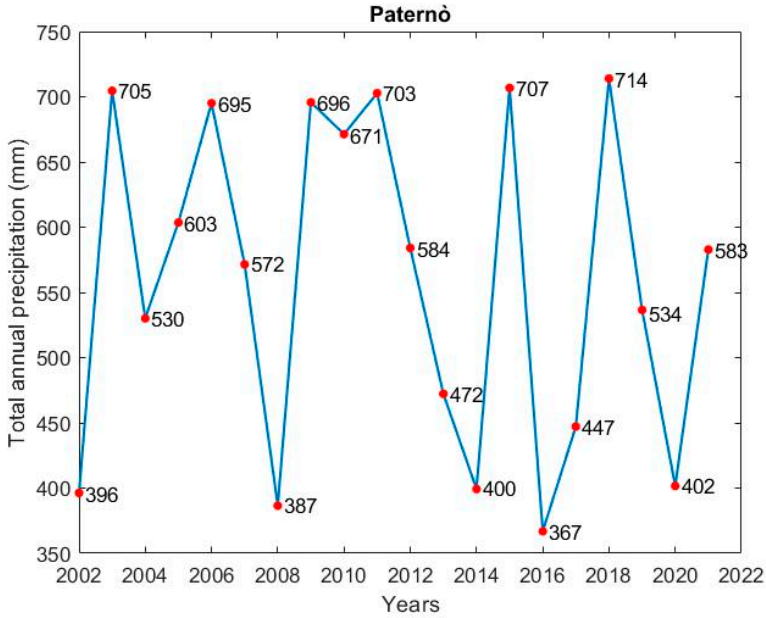
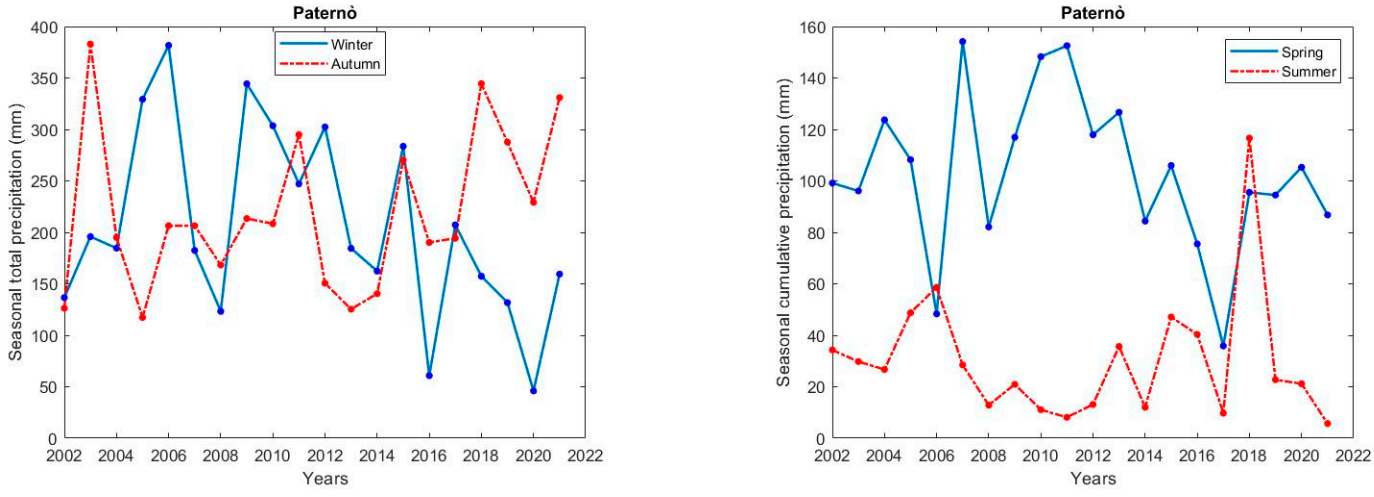


Figure 3. Trend of cumulative annual precipitation (mm) over the past twenty years (2002–2021) for the Paternò case study.

From Figure 3 it would appear that although the trend falls within a given statistical variability over the last twenty years, starting in 2014 there seem to be more frequent years when precipitation is low. It is useful then to analyze seasonal trends to understand whether precipitation trends have seasonal sensitivity, hence Figure 4a,b are shown, for the Paternò case study.



(**a**) (**b**)

Figure 4. Seasonal cumulative precipitation trends: (**a**) in winter and autumn, (**b**) in spring and summer, for the Paternò case study.

From the above figures, the cumulative amount of winter precipitation has experienced a marked reduction, portending dry spells in future years this season that could impact energy production from hydroelectric plants afferent to the Paternò catchment. Cumulative autumn precipitation has experienced an increase over the past twenty years, although with a different slope than in winter. Regarding the spring trend, a reduction can be observed from 2011 onwards, but without a marked trend as observed in winter and autumn. Finally, a decreasing trend is noted in summer, with 2018 experiencing a particularly rainy summer (probably an outlier).

In addition to the cumulative amount of seasonal and annual precipitation, it is useful to analyze trends in hourly intense precipitation events across seasons and years. Figure 5 shows annual, winter, and autumn trends of heavy precipitation. The summer trend is not shown being that in twenty years there has been no intense hourly rainfall, while the spring trend is not shown because the amount of data available does not allow inferring any trend for this season.

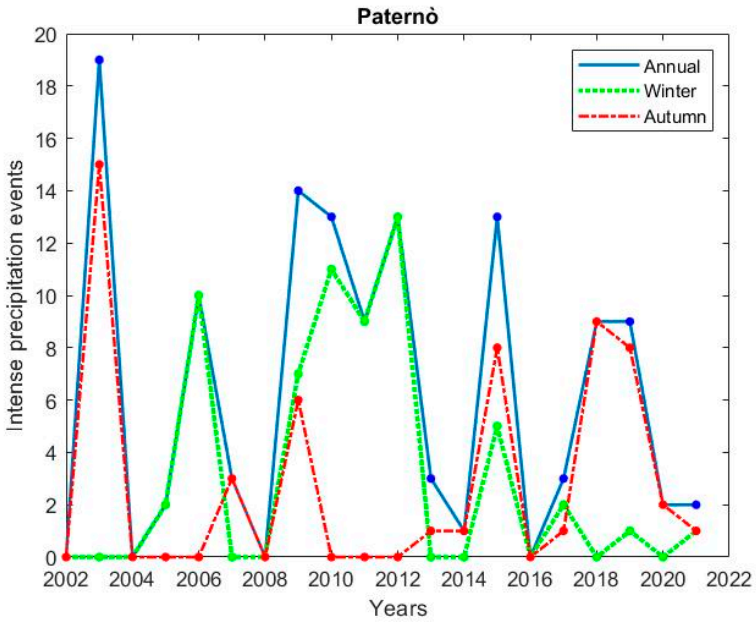


Figure 5. Trends in the number of hours (events) with intense precipitation (greater than 3.6 mm/h), on an annual basis and on a seasonal basis (winter and autumn), for the Paternò case study.

From Figure 5, in the last twenty years, the number of annual events with heavy precipitation seems to represent an increasing trend. Specifically, looking at the data from 2002 to 2010, there have been three years in which no intense precipitation occurred in any hour, while from 2010 until 2021 only one year (2016) recorded zero hourly intense precipitation. On the other hand, looking at the seasonal trend of heavy hourly precipitation, winter turns out to be the season with the highest density of hours with heavy precipitation, which from 2010 onward seems to have decreased compared to previous years. In contrast, the autumn pattern shows an increasing trend, which is likely to maintain this slope in the next years. A peak in the number of intense precipitation occurred in 2003: above-average air temperatures in the summer of 2003 probably led to an increase in the amount of water the atmosphere can hold, and thus to more frequent intense precipitation in the autumn.

The procedure carried out for Paternò is repeated for Busachi; Figure 6 shows the annual cumulative precipitation trend.

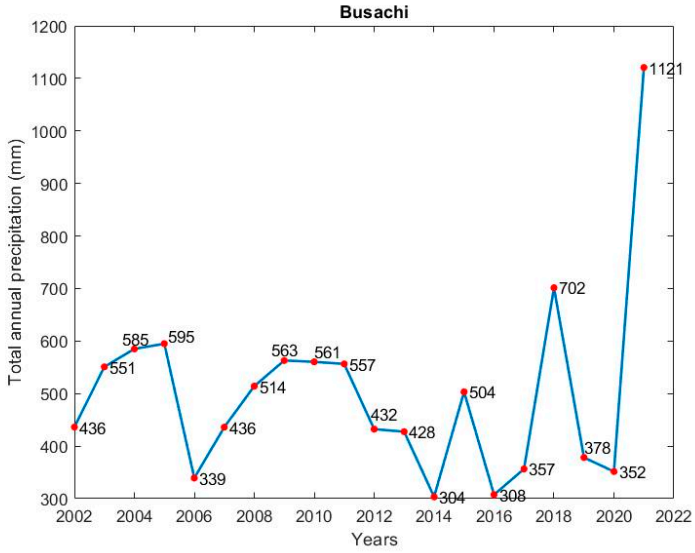
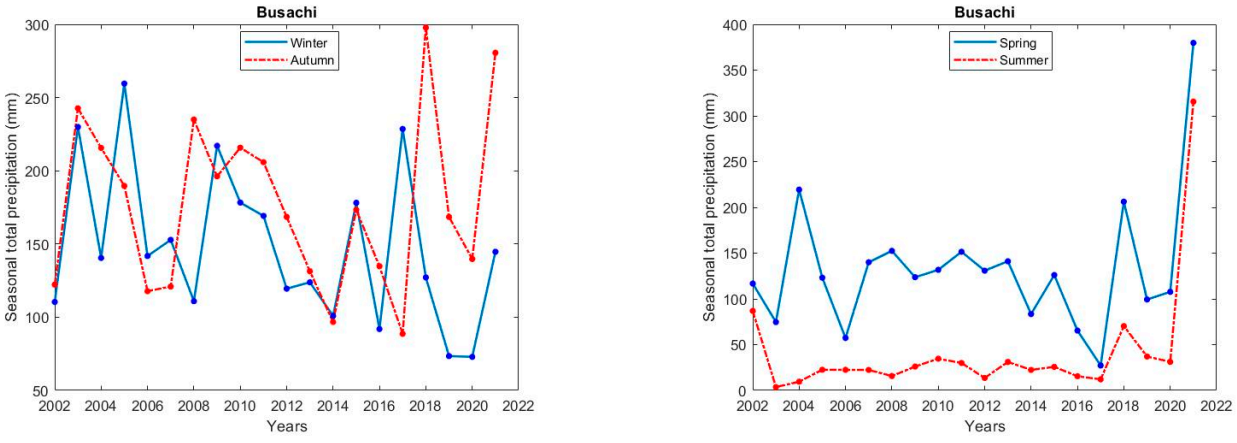


Figure 6. Trend of cumulative annual precipitation (mm) over the past twenty years (2002–2021) for the Busachi case study.

As in Paternò, there seems to be a reduction in precipitation patterns for Busachi: starting in 2014 a lack of smoothness in the trend of interannual cumulative precipitation is observed.

Now, it is useful to look at seasonal trends to see what the contribution of individual seasons might be to the overall annual contribution. Figure 7a,b shows the cumulative seasonal precipitation trends.



(**a**) (**b**)

Figure 7. Seasonal cumulative precipitation trends: (**a**) in winter and autumn, (**b**) in spring and summer, for the Busachi case study.

Figure 7a shows how Busachi has experienced a reduction in winter cumulative precipitation over the past twenty years, while in autumn an increase has been experienced. Although the cumulative precipitation values for these two seasons are slightly lower than those of Paternò, the same trends are observed for both Busachi and Paternò. Turning then to Figure 7b, the spring and summer trends both show decreasing trends, as seen for Paternò. Indeed, 2021 was a year characterized by an outsized amount of precipitation, compared to the previous nineteen years.

Regarding trends in intense precipitation, annual, spring, and autumn trends are shown in Figure 8, being that in winter no seasonal trends are observed, while in the summers of the past twenty years, there have been no heavy precipitation events.

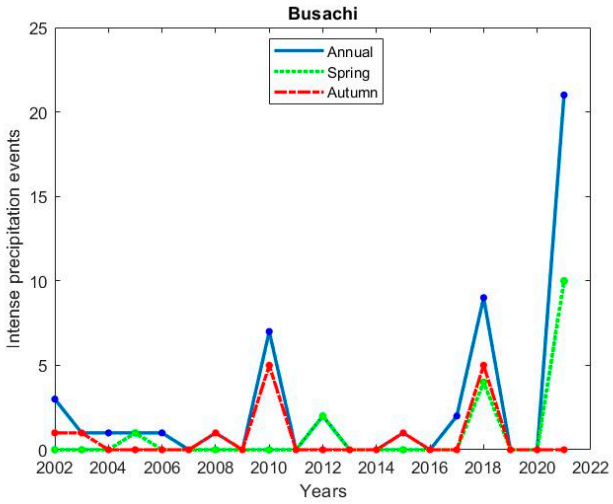


Figure 8. Trends in the number of hours (events) with intense precipitation (greater than 3.6 mm/h), on an annual basis and on a seasonal basis (spring and autumn), for the Busachi case study.

From Figure 8, there seems to be an increasing annual trend for the frequency of intense precipitation events. On the other hand, regarding seasonal trends, the frequency of intense precipitation seems to increase in autumn, and this partly explains the increase in cumulative autumn precipitation across the years. In spring there seems to be a crescendo of extreme precipitation events with a cadence of a few years.

3.3. Monte Carlo Approaches

In this subsection, results of stochastic time series generation of precipitation, runoff, and SMC are presented. Fifty Monte Carlo simulations are carried out for each of these physical quantities, and for each of these simulations, the errors in the mean and standard deviation are calculated. This yields samples of the errors whose mean, median, and standard deviation are calculated and reported in the Tables below. Table 3a,b shows the error statistics on the mean and standard deviation for Paternò and Busachi, respectively.

Table 3. (a) Mean, median, and standard deviation (STD) of the errors on the mean (e_{mean}) and standard deviation e_{STD}) evaluated in the case of synthetic hourly precipitation profiles, for the Paternò case study. (b) Mean, median, and standard deviation (STD) of the errors on the mean (e_{mean}) and standard deviation (e_{STD}) evaluated in the case of synthetic hourly precipitation profiles, for the Busachi case study.

(a)

	e_{mean}(%)				e_{STD}(%)			
	Win	**Spr**	**Sum**	**Aut**	**Win**	**Spr**	**Sum**	**Aut**
Mean	2.4	3.9	4.2	2.5	2.8	4.1	4.2	2.7
Median	1.6	3.3	3.3	2.3	2.1	3.4	3.3	2.3
STD	2.2	2.8	3.4	1.7	2.7	3.1	3.5	2.1

(b)

	e_{mean}(%)				e_{STD}(%)			
	Win	**Spr**	**Sum**	**Aut**	**Win**	**Spr**	**Sum**	**Aut**
Mean	2.7	3.4	6.0	3.3	3.6	3.3	5.9	3.5
Median	2.3	2.7	4.9	2.8	2.8	2.8	4.4	3.1
STD	2.0	2.5	4.3	2.6	3.1	2.6	5.0	2.9

The narrow values of error statistics show that the approach based on Pearson's family of distributions appropriately simulates the statistical and physical variability of historical precipitation values, for both locations.

Once the hourly synthetic precipitation profiles are obtained, they can be used as inputs to the equations for direct runoff assessments. Equation (8) is a linear combination of the precipitation values, so it is expected that the error statistics on the means and standard deviations would give results very close to those of precipitation. Regarding the direct runoff evaluated by (9), this equation binds the direct runoff nonlinearly with the precipitation, therefore, it could be expected that in this case, the results of the error statistics of the synthetic runoff profiles could deviate from the error statistics results of synthetic precipitation profiles. Table 4a,b shows the results obtained for the direct runoff with both the Rational and the NRCS methods, for the Paternò and Busachi case studies, respectively.

Table 4. (a) Mean, median, and standard deviation (STD) of the errors on the mean (e_{mean}) and standard deviation (e_{STD}) evaluated in the case of synthetic runoff profiles, for the Paternò case study. (b) Mean, median, and standard deviation (STD) of the errors on the mean (e_{mean}) and standard deviation (e_{STD}) evaluated in the case of synthetic runoff profiles, for the Busachi case study.

(a)								
Rational method								
	e_{mean}(%)				**e_{STD}(%)**			
	Win	**Spr**	**Sum**	**Aut**	**Win**	**Spr**	**Sum**	**Aut**
Mean	2.4	3.9	4.3	2.6	2.9	4.1	4.2	2.7
Median	1.5	3.2	3.3	2.3	2.1	3.5	3.3	2.3
STD	2.3	2.8	3.3	1.7	2.6	3.1	3.5	2.1
NRCS method								
	e_{mean}(%)				**e_{STD}(%)**			
	Win	**Spr**	**Sum**	**Aut**	**Win**	**Spr**	**Sum**	**Aut**
Mean	1.6	0.5	0.2	2.3	41.2	42.6	47.8	38.1
Median	0.8	0.4	0.1	1.9	42.7	43.3	49.2	38.5
STD	1.8	0.4	0.2	1.5	7.3	7.5	6.8	6.3
(b)								
Rational method								
	e_{mean}(%)				**e_{STD}(%)**			
	Win	**Spr**	**Sum**	**Aut**	**Win**	**Spr**	**Sum**	**Aut**
Mean	2.6	4.7	5.8	3.2	3.5	5.6	5.8	3.3
Median	2.2	2.5	4.5	2.8	2.7	3.0	4.2	3.1
STD	2.2	8.3	4.3	2.4	3.0	13.9	5.1	2.7
NRCS method								
	e_{mean}(%)				**e_{STD}(%)**			
	Win	**Spr**	**Sum**	**Aut**	**Win**	**Spr**	**Sum**	**Aut**
Mean	0.6	1.1	0.7	1.3	44.4	44.8	47.8	42.6
Median	0.5	0.6	0.1	1.1	44.8	44.3	47.3	42.5
STD	0.4	2.0	2.9	0.8	5.3	10.7	10.3	5.5

The synthetic profiles of the direct runoff evaluated by the Rational method show error statistics very close in magnitude to those obtained for precipitation, with two exceptions for Busachi, i.e., the STD of the error on the mean and standard deviation in spring. In contrast, in the case of the NRCS method, the synthetic direct runoff error statistics provided better results on the mean than the synthetic precipitation, in both case studies. However, the error statistics on standard deviation give results that are an order of magnitude greater than the respective statistics of the synthetic precipitation profiles, and then of the synthetic runoff profiles (Rational method). This fact could be due to the nonlinear nature of the link between precipitation and direct runoff expressed by the NRCS equation.

Regarding the synthetic generation of daily SMC profiles, the historical daily values of the specific seasons of the specific year are considered as data base. This implies that the synthetic generation algorithm is applied on significantly less data than hourly precipitation data. Table 5a,b shows the results obtained.

Table 5. (a) Mean, median, and standard deviation (STD) of the errors on the mean (e_{mean}) and the standard deviation (e_{STD}) evaluated in the case of synthetic soil moisture daily profiles, for the Paternò case study, using data of individual seasons of individual years. (b) Mean, median, and standard deviation (STD) of the errors on the mean (e_{mean}) and standard deviation (e_{STD}) evaluated in the case of synthetic soil moisture daily profiles, for the Busachi case study, using data of individual seasons of individual years.

(a)

	e_{mean}(%)				e_{STD}(%)			
	Win	**Spr**	**Sum**	**Aut**	**Win**	**Spr**	**Sum**	**Aut**
Mean	3.1	4.1	1.2	3.7	19.2	11.4	33.3	17.1
Median	2.8	4.0	1.2	3.6	10.3	7.6	20.4	13.9
STD	1.8	1.1	0.9	1.7	23.8	11.9	32.0	16.4

(b)

	e_{mean}(%)				e_{STD}(%)			
	Win	**Spr**	**Sum**	**Aut**	**Win**	**Spr**	**Sum**	**Aut**
Mean	2.6	3.2	2.2	2.9	31.8	15.9	28.0	33.7
Median	2.4	3.0	2.2	3.0	15.2	13.8	20.6	19.4
STD	1.5	1.0	1.2	1.4	34.7	12.6	26.2	31.5

The error statistics on the mean reveal little deviation between the historical and simulated averages, for both locations, comparable even with the statistics obtained in the case of precipitation; on the other hand, the error statistics on the standard deviation are higher than those on the mean, even by an order of magnitude, as in summer in Paternò, and winter, spring, autumn in Busachi. These statistics of the error on the standard deviation may or not be considered acceptable depending on the objectives of a given research work: for the purposes of this paper, the percentage values of these statistics are considered acceptable. Furthermore, it is desired to understand whether, by considering more data for generating synthetic profiles of SMC, results in lower percentage errors on the standard deviation than in the previous case. For this purpose, for each season, historical data from all twenty years of data for that season are considered, thus creating four databases, one for each season. Table 6a,b shows the results obtained.

Table 6. (a) Mean, median, and standard deviation (STD) of the errors on the mean (e_{mean}) and standard deviation (e_{STD}) evaluated in the case of synthetic soil moisture daily profiles, for the Paternò case study, using twenty years of data for each individual season. (b) Mean, median, and standard deviation (STD) of the errors on the mean (e_{mean}) and standard deviation (e_{STD}) evaluated in the case of synthetic soil moisture daily profiles, for the Busachi case study, using twenty years of data for each individual season.

(a)

	e_{mean}(%)				e_{STD}(%)			
	Win	**Spr**	**Sum**	**Aut**	**Win**	**Spr**	**Sum**	**Aut**
Mean	5.9	6.4	1.6	2.5	8.1	7.7	30.5	16.6
Median	5.7	6.3	1.4	2.5	6.3	7.0	24.1	15.6
STD	1.6	1.2	1.0	1.2	6.7	5.3	26.7	9.9

(b)

	e_{mean}(%)				e_{STD}(%)			
	Win	**Spr**	**Sum**	**Aut**	**Win**	**Spr**	**Sum**	**Aut**
Mean	2.4	3.2	2.2	3.1	21.3	12.3	26.4	36.2
Median	2.3	3.1	2.3	2.8	13.8	7.4	24.6	28.4
STD	1.4	1.0	1.1	1.6	24.1	12.5	21.7	30.1

Looking at the errors statistics on the mean in Table 6a, it can be seen that a slight improvement in percentage values is observed for autumn, while a slight increase in percentage values is observed for the other seasons. On the other hand, percentage values of the error statistics on the standard deviation show marked improvements for all seasons, especially for winter and spring. For the Busachi case study (Table 6b), there are no significant changes in the error statistics on the mean compared to when there were fewer data in the database. On the other hand, the error statistics on the standard deviation show important reductions in the percentage values for winter and spring (as in Paternò), with improvements in summer as well; autumn turns out to be the only season to show slight worsening, the only worsening outcome between the two localities, compared to Table 5a,b.

4. Discussion

There are only a few contributions in the literature on modelling hydropower generation as a function of meteorological and hydrological variables in the context of adequacy analyses. This paper attempts to fill this gap in the literature by providing tools for modelling water availability for power generation using statistical methods.

The results obtained suggest that the Monte Carlo approaches applied may be suitable for simulating hourly values of water availability for hydropower generation. Indeed, by creating synthetic precipitation profiles, hourly synthetic profiles of direct runoff can be obtained, considering either the intensity of the precipitation or its accumulated amount. These simulated hourly profiles can thus be used as input for conducting adequacy analyses. In fact, simulations of hourly profiles of water availability can be used as input to hydropower generation models, thereby simulating hourly profiles of hydropower generation for adequacy analyses by researchers and transmission system operators. In addition, this approach can be used to simulate several years of hydropower plant operation, so that different possible scenarios can be considered in each simulated year with an acceptable computational effort. In this way, both researchers and transmission system operators can understand the limits within which a given hydropower plant can elastically provide its availability to meet energy demand in a given region characterized by a specific climate, thus improving the adequacy level of the market area in which the power plants are located. Furthermore, the method proposed here can be applied to hydropower plants with reservoirs of any size and flow rate. For plants that belong to low- extent catchments, the

Rational Method is well-suited, while for plants that belong to extensive catchments, the NRCS method can be chosen.

Regarding the results of the linear regressions presented in Section 3, the strong positive correlation found for both sites in winter can be explained by the fact that winter is modelled for the months of December, January, and February and the greater amount of precipitation that accumulates in the soil in December and January meets higher radiation intensity and temperatures in February. Indeed, more water is available to the soil for evapotranspiration due to the late winter precipitation, and more ET_0 is available due to the higher irradiance and temperatures. The strong anti-correlation found for spring could be justified by the fact that irradiance and air temperature increase during this season, decreasing SMC on the one hand and increasing ET_0 on the other. A strong anti-correlation was also found for autumn, but this is probably due to different physical reasons than in the case of spring. In fact, the values for irradiance and ambient temperature decrease during this season, leading in parallel to a decrease in ET_0 and an increase in the residence time of water in the soil.

The results for the summer season, however, deserve separate consideration. The different statistical character of the results for this season could be due to the fact that in summer most SMC daily values correspond to the wilting point, the amount of water not available for evaporation and transpiration, which introduces a bias into the data thus rendering meaningless the attempt to obtain statistically significant results. Indeed, inconsistency in the sign and modulus of the correlation coefficients was found between years and between the two sites.

Finally, the fact that the coefficients of the fitting lines in the respective seasons (for all twenty years of data) for the two sites showed consistency in modulus and sign suggests that the fitting line found for the Paternò case study could also fit the Busachi case study and vice versa, although there is a difference in latitude of almost 3° between these two sites. This fact can be justified by the fact that the two places as well as the islands have the same climate. This makes it possible to claim that through the empirical relationships derived here, diurnal profiles of ET_0 can be estimated from SMC diurnal data for other regions that share the same climate with the places analyzed here and whose soil textures are typical of Mediterranean flora, albeit at somewhat different latitudes than those of the case studies in this paper. The added advantage of these empirical relationships is that ET_0 profiles can be obtained for a given weather-simulated season or year using daily SMC values as input, without having to use formulae that consider meteorological data that are not always available from satellite or in situ measurements.

Analyses of seasonal and annual hourly rainfall trends, as well as evaluation of the number of extreme rainfall events, suggest that there is less precipitation in Busachi than in Paternò. This fact has implications for the statistical significance of Busachi's historical data in terms of intense rainfall events, which are rarer in Busachi and require a longer time span than the twenty years considered (although all hourly rainfall data available in [28] were used). Finally, the historical hourly precipitation profiles show that the cumulative precipitation amounts tend to decrease on an annual and seasonal basis at both locations studied (with the exception of autumn, where a slight increase is observed). These observations are consistent with several scientific papers that use climate model projections to define the Mediterranean as a hotspot of global warming, with a significant increase in air temperature values and increasingly frequent and prolonged droughts [18]. As the amount of precipitation in the Mediterranean decreases, hydropower generation is increasingly constrained, leading to an increased risk of inadequate power systems in the various Mediterranean countries. Future research must therefore address the analysis of historical precipitation trends in Mediterranean countries and future climate projections for precipitation patterns so that power system operators can plan effective responses to this problem in the medium and long term.

As for the Monte Carlo simulations, the synthetic hourly precipitation profiles reproduced well the statistical properties of the historical hourly profiles for both sites. Since

the approach used for the synthetic generation of hourly profiles relies on statistics calculated from historical data, it can be concluded that statistically significant results can also be obtained for sites other than those considered in this paper. For the synthetic hourly profiles of direct runoff, the results obtained with the NRCS method show an order of magnitude larger standard deviation than the standard deviation of the profiles obtained with the Rational method. This can be justified by the fact that in the Rational method, the relationship between precipitation and direct runoff is linear, whereas in the NRCS method, it is non-linear.

Regarding the synthetic generation of SMC daily profiles, it can be noted that overall significant improvements in the percentage values of standard deviation errors are obtained when all twenty years of available data for each season are used, compared to using data from only one year for the generation of SMC synthetic profiles. Future research should use the results of the synthetic profiles of the meteorological and hydrological variables obtained here as input for simulations of the hourly profiles of the active power generated by hydroelectric plants at the sites selected as case studies.

5. Conclusions

In this paper statistical approaches to assess water availability in the context of hydropower generation and adequacy analysis on a seasonal basis are applied, two Italian locations are considered for the numerical analysis, one in Sicily and the other in Sardinia, where major hydroelectric plants are present. First, an empirical relationship between soil moisture content (SMC) and potential evapotranspiration (ET0) is evaluated through linear regression analysis. Linear regression carried out with first-degree polynomials yielded fitting lines whose coefficients have the consistency of magnitude and sign in both case studies. This fact, in addition to the high values obtained from Spearman's correlation coefficient and the R^2 coefficient, suggests that the fitting lines evaluated in this work can be used to estimate ET_0 from SMC data (publicly available), for geographic areas affected by the Mediterranean climate.

Analyses of precipitation trends showed that at both locations there has been a reduction in cumulative precipitation over the past twenty years, with decreasing trends in winter and summer. It is expected that these trends will be confirmed in the years to come, and prolonged periods of drought in critical seasons for energy demand such as winter and summer may lead to major reductions in water availability, and thus hydropower production, with consequent adequacy risks for the Sicily and Sardinia market zones.

Finally, Monte Carlo algorithms, applied to generate synthetic profiles of precipitation, direct runoff, and SMC, have proven successful in capturing the statistical variability of historical data of these meteorological quantities. Thus, through the synthetic profiles of water availability obtained in this work, stochastic analyses of hydropower production can be conducted for the purpose of the assessment of the adequacy of an electric power system.

Future research should continue in this direction, including modeling snow as a natural reservoir of water availability for hydropower production, and conducting adequacy analyses on a seasonal basis, since weather quantities have marked inter-seasonal variability that impacts electricity generation and demand in different ways depending on the season.

Author Contributions: Conceptualization, G.M.T. and C.F.N.; methodology, G.M.T. and C.F.N.; software, G.M.T.; validation G.M.T. and C.F.N.; formal analysis, G.M.T. and C.F.N.; investigation, C.F.N. and G.M.T.; data curation, C.F.N.; writing—original draft preparation, C.F.N. and G.M.T.; writing—review and editing, G.M.T.; visualization, C.F.N.; supervision, G.M.T. All authors have read and agreed to the published version of the manuscript.

Funding: This research received no external funding.

Institutional Review Board Statement: Not applicable.

Informed Consent Statement: Not applicable.

Data Availability Statement: The data used for this study are available online (open access) at the following site of a NASA project: https://power.larc.nasa.gov/, accessed on 20 December 2022.

Conflicts of Interest: The authors declare no conflict of interest.

References

1. Neelin, J. *Climate Change and Climate Modeling*; Cambridge University Press: Cambridge, UK, 2010. [CrossRef]
2. WMO. "Climate" WMO. 2021. Available online: https://public.wmo.int/en/our-mandate/climate (accessed on 23 November 2021).
3. IPCC. *Climate Change 2021, The Physical Science Basis*; IPCC: Geneva, Switzerland, 2021.
4. IEA-International Energy Agency. CO2 Emissions. 2021. Available online: https://www.iea.org/reports/global-energy-review-2021/co2-emissions (accessed on 29 November 2021).
5. European Environment Agency. Greenhouse Gas Emissions by Aggregated Sector. 19 December 2019. Available online: https://www.eea.europa.eu/data-and-maps/daviz/ghg-emissions-by-aggregated-sector-5/#tab-dashboard-02 (accessed on 10 January 2022).
6. European Environment Agency. Greenhouse Gas Emission Intensity of Electricity Generation in Europe. 18 November 2021. Available online: https://www.eea.europa.eu/ims/greenhouse-gas-emission-intensity-of-1 (accessed on 10 January 2022).
7. Eurostat. Renewable Energy Statistics. EU, 08 01 2022. Available online: https://ec.europa.eu/eurostat/statistics-explained/index.php?title=Renewable_energy_statistics (accessed on 10 January 2022).
8. Hydropower-Europe. Hydropower in Europe. *Hydropower-Europe-EU*. 2020. Available online: https://hydropower-europe.eu/about-hydropower-europe/hydropower-energy/ (accessed on 10 January 2022).
9. European Commision. *The European Green Deal*; EU-Commission: Brussels, Belgium, 2019.
10. European Commission. *REPowerEU Plan*; EU-Commission: Brussels, Belgium, 2022.
11. European Commission. *'Fit for 55': Delivering the EU's 2030 Climate Target on the Way to CLIMATE Neutrality*; EU-Commission: Brussels, Belgium, 2021.
12. Tina, G.M.; Nicolosi, C.F.; Stefanelli, D. The impacts of synthetic correlated generation of weather variables on adequacy analyses. In Proceedings of the IEEE, AEIT International Annual Conference (AEIT), Rome, Italy, 3–5 October 2022; Volume 2022, pp. 1–6. [CrossRef]
13. Tina, G.M.; Nicolosi, C.F. Assessment of the Impacts of Climate Change on Power Systems: The Italian Case Study. *Appl. Sci.* **2021**, *11*, 11821. [CrossRef]
14. Engeland, K.; Borga, M.; Creutin, J.; François, B.; Ramos, M.; Vidal, J. Space-time variability of climate variables and intermittent renewable electricity production—A review. *Renew. Sustain. Energy Rev.* **2017**, *79*, 600–617. [CrossRef]
15. Dubey, S.; Sarvaiya, J.N.; Seshadri, B. Temperature Dependent Photovoltaic (PV) Efficiency and Its Effect on PV Production in the World—A Review. *Energy Procedia* **2013**, *33*, 311–321. [CrossRef]
16. Bloomfield, H.C.; Brayshaw, D.J.; Troccoli, A.; Goodess, C.M.; De Felice, M.; Dubus, L.; Bett, P.E.; Saint-Drenan, Y.M. Quantifying the sensitivity of european power systems to energy scenarios and climate change projections. *Renew. Energy* **2021**, *164*, 1062–1075. [CrossRef]
17. Panteli, M.; Mancarella, P. Influence of extreme weather and climate change on the resilience of power systems: Impacts and possible mitigation strategies. *Elsevier Electr. Power Sytems Res.* **2015**, *127*, 259–270. [CrossRef]
18. Gao, X.; Giorgi, F. Increased aridity in the Mediterranean region under greenhouse gas forcing estimated from high resolution simulations with a regional climate model. *Glob. Planet. Change* **2008**, *62*, 195–209. [CrossRef]
19. Tobin, I.; Greuell, W.; Jerez, S.; Ludwing, F.; Vautard, R.; van Vliet, M.T.H.; Bréon, F.M. Vulnerabilities and resilience of European power generation to 1.5 °C, 2 °C and 3 °C warming. IOP Science-Environ. *Res. Lett.* **2018**, *13*, 044024. [CrossRef]
20. Jacob, D.; Kotova, L.; Teichmann, C.; Sobolowski, S.P.; Vautard, R.; Donnelly, C.; Koutroulis, A.G.; Grillakis, M.G.; Tsanis, I.K.; Damm, A.; et al. Climate Impacts in Europe Under +1.5 °C Global Warming. *AGU-Adv. Earth Space Sci. Earth's Future* **2018**, *6*, 264–285. [CrossRef]
21. European commission. EU Action to Address the Energy Crisis. EU. 2022. Available online: https://commission.europa.eu/strategy-and-policy/priorities-2019-2024/european-green-deal/eu-action-address-energy-crisis_en (accessed on 14 January 2023).
22. Härtel, P.; Korpås, M. Aggregation Methods for Modelling Hydropower and Its Implications for a Highly Decarbonised Energy System in Europe. *Energies* **2017**, *10*, 1841. [CrossRef]
23. Notton, G. Importance of islands in renewable energy production and storage: The situation of the French islands. *Renew. Sustain. Energy Rev.* **2015**, *47*, 260–269. [CrossRef]
24. Abadie, L.M.; Chamorro, J.M.; Huclin, S. van de Ven Dirk-Jan. On flexible hydropower and security of supply: Spain beyond 2020. *Energy* **2020**, *203*, 117869. [CrossRef]
25. Huertas-Hernando, D.; Farahmand, H.; Holttinen, H.; Kiviluoma, J.; Rinne, E.; Söder, L.; Milligan, M.; Ibanez, E.; Martinez, S.M.; Gómez-Lázaro, E.; et al. Hydropower Flexibility for Power Systems with Variable Renewable Energy Sources. In *Advances in Energy Systems: The Large-scale Renewable Energy Integration Challenge*; Peter, D.L., John, B., Reinhard, H., Damian, F., Eds.; Wiley: Hoboken, NJ, USA, 2019; pp. 385–405. [CrossRef]
26. Khalilzadeh, E.; Fotuhi-Firuzabad, M.; Aminifar, F.; Ghaedi, A. Reliability Modeling of Run-of-the-River Power Plants in Power System Adequacy Studies. *IEEE Trans. Sustain. Energy* **2014**, *5*, 1278–1286. [CrossRef]

27. Lambert, F.H.; Stine, A.R.; Krakauer, N.Y.; Chiang, J.C.H. How Much Will Precipitation Increase With Global Warming? *Eos. Trans. Am. Geophys. Union* **2008**, *89*, 193–194. [CrossRef]
28. Salzmann, M. Global warming without global mean precipitation increase? *Sci. Adv.* **2016**, *2*, e1501572. [CrossRef]
29. NASA. The POWER Project–NASA Langley Research Center (LaRC) POWER Project. NASA Earth Science/Applied Science Program. 2022. Available online: https://power.larc.nasa.gov/ (accessed on 20 December 2022).
30. Park, G.T.; An, S.-H.; Jang, D.-W. Runoff Estimation in Ungauged Watershed and Sensitivity Analysis According to the Soil Characteristics: Case Study of the Saint Blaise Vallon in France. *Sustainability* **2022**, *14*, 9848. [CrossRef]
31. Bonan, G. Water Balance. In *Ecological Climatology: Concepts and Applications, Cambridge*; Cambridge University Press: Cambridge, UK, 2015; pp. 155–172. [CrossRef]
32. Rai, R.K.; Singh, V.P.; Upadhyay, A. Chapter 17—Soil Analysis. In *Planning and Evaluation of Irrigation Projects*; Academic Press: Cambridge, MA, USA, 2017; pp. 505–523. [CrossRef]
33. Bonan, G. Soil Physics. In *Ecological Climatology: Concepts and Applications, Cambridge*; Cambridge University Press: Cambridge, UK, 2015; pp. 143–154. [CrossRef]
34. Davie, T. *Fundamentals of Hydrology*, 3rd ed.; Routledge: London, UK, 2019. [CrossRef]
35. Wang, Y.; Zhang, Y.; Yu, X.; Jia, G.; Liu, Z.; Sun, L.; Zheng, P.; Zhu, X. Grassland soil moisture fluctuation and its relationship with evapotranspiration. *Ecol. Indic.* **2021**, *131*, 108196. [CrossRef]
36. Shuttleworth, W.J. Evaporation. Maidment, D.R., Ed.; In *Handbook of Hydrology*; McGraw-Hill Inc.: New York, NY, USA, 1993; pp. 4.1–4.53.
37. Paredes, P.; Pereira, L.S.; Almorox, J.; Darouich, H. Reference grass evapotranspiration with reduced data sets: Parameterization of the FAO Penman-Monteith temperature approach and the Hargeaves-Samani equation using local climatic variables. *Agric. Water Manag.* **2020**, *240*, 106210. [CrossRef]
38. Hargreaves, G.H.; Samani, Z.A. Estimating Potential Evapotranspiration. *J. Irrig. Drain. Div.* **1982**, *108*, 225–230. [CrossRef]
39. Hargreaves, G.H. Defining and Using Reference Evapotranspiration. *J. Irrig. Drain. Eng.* **1994**, *120*, 1132–1139. [CrossRef]
40. Berti, A.; Tardivo, G.; Chiaudani, A.; Rech, F.; Borin, M. Assessing reference evapotranspiration by the Hargreaves method in north-eastern Italy. *Agric. Water Manag.* **2014**, *140*, 20–25. [CrossRef]
41. Gentilucci, M.; Bufalini, M.; Materazzi, M.; Barbieri, M.; Aringoli, D.; Farabollini, P.; Pambianchi, G. Calculation of Potential Evapotranspiration and Calibration of the Hargreaves Equation Using Geostatistical Methods over the Last 10 Years in Central Italy. *Geosciences* **2021**, *11*, 348. [CrossRef]
42. Samani, Z. Estimating Solar Radiation and Evapotranspiration Using Minimum Climatological Data. *J. Irrig. Drain. Eng.* **2000**, *126*, 265–267. [CrossRef]
43. Bloomfield, H.C.; Brayshaw, D.J.; Shaffrey, L.C.; Coker, P.J.; E Thornton, H. Quantifying the increasing sensitivity of power systems to climate variability. *Environ. Res. Lett. IOP Sci.* **2016**, *11*, 124025. [CrossRef]
44. Knerr, I.; Trachte, K.; Garel, E.; Huneau, F.; Santoni, S.; Bendix, J. Partitioning of Large-Scale and Local-Scale Precipitation Events by Means of Spatio-Temporal Precipitation Regimes on Corsica. *Atmosphere* **2020**, *11*, 417. [CrossRef]
45. United States Department of Agriculture—Natural Resources Conservation Service. Chapter 10—Estimation of Direct Runoff from Storm Rainfall. in Part 630—Hydrology—National Engineering Handbook, United States Department of Agriculture. 2004; pp. 1–79. Available online: https://directives.sc.egov.usda.gov/OpenNonWebContent.aspx?content=17752.wba (accessed on 6 December 2022).
46. Ponce, V.M.; Hawkins, R.H. Runoff Curve Number: Has It Reached Maturity? *J. Hydrol. Eng.* **1996**, *1*, 11–19. [CrossRef]
47. Clapp, R.B.; Hornberger, G.M. Empirical equations for some soil hydraulic properties. *Water Resour. Res.* **1978**, *14*, 601–604. [CrossRef]

Disclaimer/Publisher's Note: The statements, opinions and data contained in all publications are solely those of the individual author(s) and contributor(s) and not of MDPI and/or the editor(s). MDPI and/or the editor(s) disclaim responsibility for any injury to people or property resulting from any ideas, methods, instructions or products referred to in the content.